An Improved Sensorless IPMSM Control at Low speeds and Standstill for Washing Machine Drives Using dsPIC Technology

M. Bourogaoui*, H. Ben Attia Sethom*, I. Slama-Belkhodja, H. Sammoud*****

**Université de Carthage, Ecole Supérieure de Technologie et d'Informatique, 2035, Tunis, Tunisie ; e-mail: belhajbrahimolfa@yahoo.fr*
***Université de Tunis El Manar, Ecole Nationale d'Ingénieurs de Tunis, LR11ES15 Laboratoire des Systèmes Electriques, 1002, Tunis, Tunisie ;*
****APPCON Technologies SUARL, Parc Technologique B.P.130, 2088, Ariana, Tunisie.*

Abstract: The purpose of this paper is to present an improved position estimation method without mechanical sensor. This method, based on the Alternating Voltage Injection (AVI) technique, is applied for washing machines with Interior Permanent Magnet Synchronous Motor (IPMSM). To validate the effectiveness of the proposed method, both comprehensive simulations using MATLAB/Simulink® and experimental results were conducted using a 1kW IPMSM designed for washing machines under different speed conditions.
The improved position estimation method was implemented using a fast digital signal processor (dsPIC30F6010A).
The obtained results highlight the advantages of the proposed technique at low speeds and standstill. Indeed, the improved position estimation method offers an estimated average position error within 2°.
The paper describes an improved position estimation method at low speeds and standstill. The proposed sensorless control scheme does not require an extra hardware or huge memory space for real time implementation.

Keywords: Interior Permanent Magnet Synchronous Motor (IPMSM), Low speeds, Standstill, Shifted High Frequency (SHF) current demodulation, Washing Machine Drive.

1. INTRODUCTION

In recent years, the variable speed control of Interior Permanent Magnet Synchronous Motors (IPMSM) is applied in modern domestic washing machine drives, where the motor works at low speeds and large dynamic torque levels during the tumble-wash cycle. In addition, position sensors associated to IPMSM drives are subject to high level mechanical vibrations, noise and load torque variations, due to the washing machines operating at different washing cycles. Moreover, for such applications, position sensors associated to IPMSM drives are the most expensive and delicate components compared to motors, converters, current sensors and control tools. Then, the use of position estimation techniques is required to reduce the washing machines cost, and improve the performance of their drives, (BelHadj Brahim et al., 2011, a; Balazovic et al., 2008; Andreescu, 2003).

Recently, various types of high frequency signal injection based sensorless control algorithms have been performed in order to propose reliable and low-cost performance control strategies for IPMSM drives, at specific operating conditions such as low speed ranges and standstill, (Chaudhary et al., 2008; Silva et al., 2003; Villet et al., 2012; Chen et al., 2012).

High Frequency Signal Injection (HFSI) techniques may be categorized under two main groups : transient signal injection based techniques and continuous signal injection based ones. The first are based on exploiting the PWM signal to extract the rotor position or to inject discrete test voltage pulses in a defined direction (Hua et al., 2011; De Belie et al., 2010; Wang et al., 2009; Wang et al., 2004; Foo et al., 2010). The latter are based on an injection of a high frequency signal in order to excite the motor voltage supply, (BelHadj Brahim et al., 2011, b; BelHadj Brahim et al., 2012, c; BelHadj Brahim et al., 2013, d; Wallmark et al., 2012).

From experimental point of view, the techniques based on the continuous HFSI scheme are easier to be implemented than those based on the transient HFSI scheme for sensorless control of real time systems.

The different continuous signal injection techniques reported in the literature can be classified in two main groups, (BelHadj Brahim et al., 2011, b; BelHadj Brahim et al., 2012, c; BelHadj Brahim et al., 2013, d):

- ***Pulsating Voltage Injection (PVI) techniques*** that are based on an injected signal reported to a fixed high frequency voltage vector in the rotor reference frame (d,q).
- ***Alternating Voltage Injection (AVI) techniques*** which are based on an injected signal reported to a rotating high frequency voltage vector in the stator reference frame (α,β).

In the latter techniques, High Frequency (HF) current response must be processed in order to extract the IPMSM rotor position. For this purpose, three demodulation algorithm schemes have been proposed and detailed in: (BelHadj Brahim et al., 2011, b; BelHadj Brahim et al., 2012, c; BelHadj Brahim et al., 2013, d; Wallmark et al., 2012).

- ***The Heterodyning demodulation scheme*** which consists in detecting the modulated signal by multiplying it by an intermediate signal that frequency is comprised between the carrier signal frequency and the frequency of the signal to be transmitted.
- ***The Homodyning demodulation scheme*** which consists in detecting the modulated signal by multiplying it by its carrier signal.
- ***The Shifted High Frequency SHF current demodulation*** which consists in a standard demodulation of the shifted HF currents.

However, the reported demodulation schemes algorithms suffer from two main drawbacks. Indeed, these algorithms are relatively complex to be implemented and cannot ensure high performance sensorless control at low speeds and standstill.

In this paper, a modified position estimation scheme using Alternating Voltage Injection (AVI) technique and based on modified Shifted High Frequency (SHF) current demodulation is proposed in order to improve IPMSM sensorless control at low speeds and standstill.

This paper starts with a reviewing of the sensorless V/f Open Loop control strategy for IPMSM drives, and a theoretical background related to the high frequency IPMSM model developed in the stationary frame injection (α,β).

Thereafter, a modified Shifted High Frequency (SHF) current demodulation technique is proposed and detailed. Simulation and experimental results are presented and discussed in order to verify the proposed sensorless control scheme performance.

2. SENSORLESS V/f OPEN LOOP CONTROL STRATEGY FOR IPMSM DRIVES

In order to validate the rotor position estimator performance based on the modified (SHF) current demodulation technique, constant Volt per Hertz V/f Open Loop control is used for the IPMSM.

Different reference frames can be used to model the motor : three phases frame (a,b,c), stationary frame (α,β) or synchronous frame (d,q). From the control point of view, the (d,q) reference frame is widely used, (BelHadj Brahim et al., 2011, a; De Belie et al., 2010).

The permanent magnet flux is oriented along the d-axis, where the q-axis is perpendicular to the d-axis.

In the (d,q) reference frame, the stator voltage components and the stator flux expressions are given by equations (1) to (4).

$$v_{sd} = R_s i_{sd} + L_{sd} \frac{di_{sd}}{dt} - \theta_e L_{sq} i_{sq} \tag{1}$$

$$v_{sq} = R_s i_{sq} + L_{sq} \frac{di_{sq}}{dt} + \theta_e L_{sd} i_{sd} + \theta_e \Psi_f \tag{2}$$

$$\Psi_{sd} = L_{sd} i_{sd} + \Psi_f \tag{3}$$

$$\Psi_{sq} = L_{sq} i_{sq} \tag{4}$$

The electromagnetic torque is given by (5).

$$C_{em} = \frac{3}{2} p \left(\left(L_{sd} - L_{sq} \right) i_{sd} i_{sq} + \Psi_f i_{sq} \right) \tag{5}$$

In IPMSM drive, it is assumed that $L_{sq} > L_{sd}$.

The model described by equations (1) to (5) is available in the following conditions:

- The induced EMF is supposed sinusoidal.

- The magnetic circuit motor is not saturated and the rotor amortization effect is neglected.

- The air-gap irregularities due to stator notches are ignored.

- The Eddy currents and hysteresis losses are neglected.

- The stator resistances temperature effect is ignored.

Fig.1 shows a known block diagram of an IPMSM sensorless V/f Open Loop control strategy. The considered IPMSM drive includes conventional modules for V/f Open Loop control such as Clark transformation and PWM module. A rotor position estimator is added to the drive in order to perform the position estimation processing.

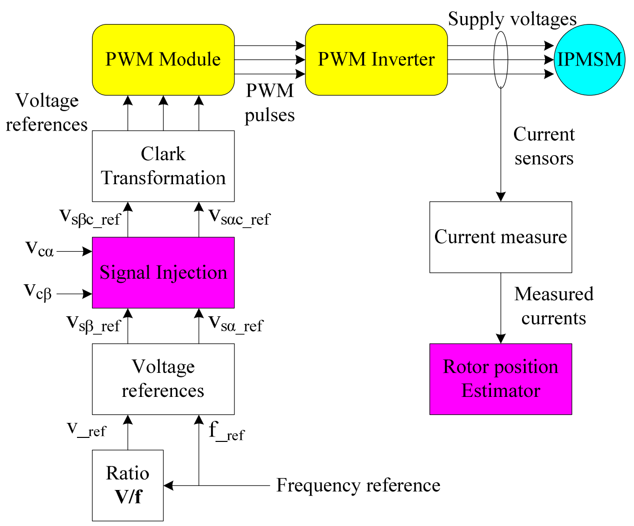

Fig. 1. IPMSM sensorless V/f Open Loop control strategy block diagram.

3. HIGH FREQUENCY IPMSM MODEL IN THE (α,β) REFERENCE FRAME

The IPMSM model is considered in the (α,β) stator reference frame. This model is available under the same conditions dictated in section 2.

The stator voltage components are presented by the following equations form (6) and (7).

$$v_{s\alpha} = R_s i_{s\alpha} + \frac{d\psi_{s\alpha}}{dt} \tag{6}$$

$$v_{s\beta} = R_s i_{s\beta} + \frac{d\psi_{s\beta}}{dt} \tag{7}$$

where

$$\Psi_{s\alpha} = \left(L_0 + L_1 \cos\left(2\theta_e\right)\right) i_{s\alpha} + L_1 \sin\left(2\theta_e\right) i_{s\beta} + \psi_f \cos\left(\theta_e\right) \tag{8}$$

$$\Psi_{s\beta} = L_1 \sin\left(2\theta_e\right) i_{s\alpha} + \left(L_0 - L_1 \cos\left(2\theta_e\right)\right) i_{s\beta} + \psi_f \sin\left(\theta_e\right) \tag{9}$$

L_0 and L_1 are defined respectively by (10) and (11):

$$L_0 = \frac{L_{sd} + L_{sq}}{2} \tag{10}$$

$$L_1 = \frac{L_{sd} - L_{sq}}{2} \tag{11}$$

As AVI techniques consist in injecting a HF voltage on the (α,β) stator voltage axis, they cause magnetic saliencies excitation (Silva et al., 2003; El Murr et al., 2007, a). Then, it results in HF voltage and current response. The HF currents and voltages can be considered in a (αc,βc) stator reference frame, which makes θ_e with the (dc,qc) rotor reference frame, as it is shown in Fig.2.

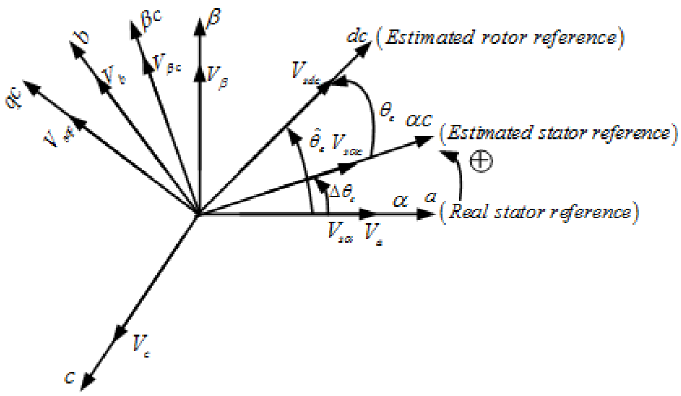

Fig. 2. The (a,b,c), the estimated (αc,βc) and the estimated (dc,qc) reference frames.

As the HF injected voltage is expressed in the (αc,βc) reference frame by equations (12) and (13),

$$v_{c\alpha} = V_{c\max} \cos\left(\omega_c t\right) \tag{12}$$

$$v_{c\beta} = -V_{c\max} \sin\left(\omega_c t\right) \tag{13}$$

Then the stator voltage equations given by (6) and (7) can be simplified by considering the following assumptions, (Andreescu, 2003; BelHadj Brahim et al., 2012, c):

- The stator resistance R_s can be neglected compared to the high frequency reactance.
- HF injected voltage pulsation ω_c is higher compared to ω_e, so ω_e is assumed to be neglected.
- The production of the back-EMF is negligible because rotor vibrations are very small.

Thus high frequency response, stator voltage is presented by the equations (14) and (15).

$$v_{s\alpha c} = j\omega_c \psi_{s\alpha c} \tag{14}$$

$$v_{s\beta c} = j\omega_c \psi_{s\beta c} \tag{15}$$

where

$v_{s\alpha c}$ and $v_{s\beta c}$ are the voltage components resulting from the AVI,

$\psi_{s\alpha c}$ and $\psi_{s\beta c}$ are the flux components resulting from the AVI.

The stator flux equations given by (8) and (9) can be simplified in the HF reference frame (αc,βc) by considering that the production of the back-EMF is negligible, since this study is intended at low speeds and standstill. Thus, stator flux equations given by (8) and (9) can be approximated in the HF reference frame respectively by (16) and (17).

$$\Psi_{s\alpha c} = L_{\alpha c} i_{s\alpha c} + L_{\alpha\beta c} i_{s\beta c} \tag{16}$$

$$\Psi_{s\beta c} = L_{\alpha\beta c} i_{s\alpha c} + L_{\beta c} i_{s\beta c} \tag{17}$$

where

$i_{s\alpha c}$ and $i_{s\beta c}$ are the current components resulting from the AVI,

$L_{\alpha c}$, $L_{\beta c}$ and $L_{\alpha\beta c}$ are respectively defined by (18), (19) and (20):

$$L_{\alpha c} = \frac{L_{sd} + L_{sq}}{2} + \frac{L_{sd} - L_{sq}}{2} \cos\left(2\theta_e\right) = L_0 + L_1 \cos\left(2\theta_e\right) \tag{18}$$

$$L_{\beta c} = \frac{L_{sd} + L_{sq}}{2} - \frac{L_{sd} - L_{sq}}{2} \cos\left(2\theta_e\right) = L_0 - L_1 \cos\left(2\theta_e\right) \tag{19}$$

$$L_{\alpha\beta c} = \frac{L_{sd} - L_{sq}}{2} \sin\left(2\theta_e\right) = L_1 \sin\left(2\theta_e\right) \tag{20}$$

As a result, the stator voltage equations given by (14) and (15) can be expressed respectively by (21) and (22).

$$v_{s\alpha c} = j\omega_c \left(L_{\alpha c} i_{s\alpha c} + L_{\alpha\beta c} i_{s\beta c}\right) \tag{21}$$

$$v_{s\beta c} = j\omega_c \left(L_{\alpha\beta c} i_{s\alpha c} + L_{\beta c} i_{s\beta c}\right) \tag{22}$$

Then, the IPMSM high frequency stator currents defined in the estimated stator reference frame (αc,βc) and resulting from (21) and (22) are given by equations (23) and (24).

$$i_{s\alpha c} = i_{cp} \cos\left(\omega_c t\right) - i_{cn} \cos\left(2\theta_e - \omega_c t\right) \tag{23}$$

$$i_{s\beta c} = i_{cp} \sin\left(\omega_c t\right) - i_{cn} \sin\left(2\theta_e - \omega_c t\right) \tag{24}$$

where

$$i_{cp} = \frac{L_0 V_{c\max}}{j\omega_c L_{sd} L_{sq}} \qquad (25)$$

$$i_{cn} = \frac{L_1 V_{c\max}}{j\omega_c L_{sd} L_{sq}} \qquad (26)$$

i_{cp} represents the positive component of the HF current vector and is proportional to the average value of the (d,q) stator inductances.

i_{cn} represents the negative component of the HF current vector and is proportional to the (d,q) inductances variation level. Starting from (23) and (24), the relations between the carrier current components, respectively $i_{s\alpha c}$ and $i_{s\beta c}$, and the rotor position θ_e are highlighted.

Then, in the next section, equations (23) and (24) will be considered in order to estimate the IPMSM rotor position.

4. MODIFIED CARRIER CURRENT DEMODULATION SCHEME

In order to extract the rotor position from (23) and (24), both $i_{s\alpha c}$ and $i_{s\beta c}$ must be demodulated. As introduced previously, it is possible to use one of the following demodulation schemes (BelHadj Brahim et al., 2012, c; BelHadj Brahim et al., 2013, d):

- Heterodyning demodulation scheme ;
- Homodyning demodulation scheme ;
- Shifted High Frequency (SHF) current demodulation scheme.

In this study, the SHF current demodulation technique is considered to estimate the rotor position and its scheme principle is described in the next subsection.

4.1 Shifted High Frequency current demodulation principle

The SHF current demodulation scheme principle is shown in Fig.3., (El Murr et al., 2007, a; El Murr et al., 2008, b; El Murr et al., 2008, c; BelHadj Brahim et al., 2013, d).

The current signals $i_{s\alpha c}$ and $i_{s\beta c}$, oscillating at the injection signal frequency f_c, are respectively obtained from $i_{s\alpha}$ and $i_{s\beta}$ using a high-pass filter (HPF). Furthermore, the real and imaginary parts of the filtered signals are delayed respectively by $-\frac{\pi}{4}$.

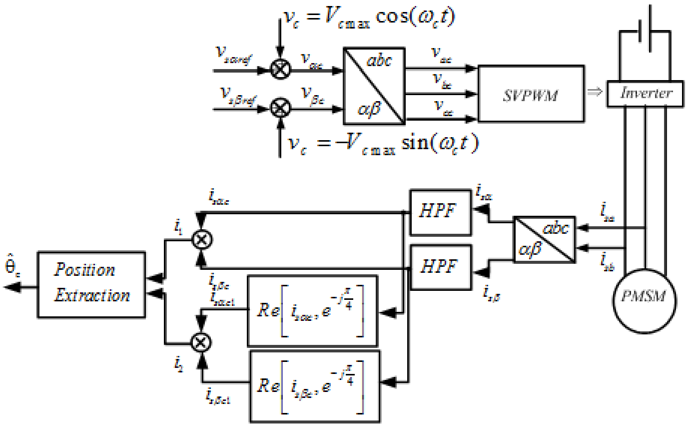

Fig. 3. IPMSM rotor position estimation scheme using SHF current demodulation based AVI technique.

Thus the obtained signals $i_{s\alpha c1}$ and $i_{s\beta c1}$ are given by equations (27) and (28).

$$i_{s\alpha c1} = \mathrm{Re}\left[i_{s\alpha c}, e^{-j\frac{\pi}{4}}\right] = i_{cp}\cos(\omega_c t - \frac{\pi}{4}) - i_{cn}\cos(2\theta_e - \omega_c t - \frac{\pi}{4}) \qquad (27)$$

$$i_{s\beta c1} = \mathrm{Re}\left[i_{s\beta c}, e^{-j\frac{\pi}{4}}\right] = i_{cp}\sin(\omega_c t - \frac{\pi}{4}) - i_{cn}\sin(2\theta_e - \omega_c t - \frac{\pi}{4}) \qquad (28)$$

The multiplication of real and imaginary parts of $i_{s\alpha c}$ and $i_{s\beta c}$ by each others results in the current i_1. As well as the multiplication of real and imaginary parts of $i_{s\alpha c1}$ and $i_{s\beta c1}$ by each others results in the current i_2. Then, the currents i_1 and i_2 are considered in order to extract the IPMSM rotor position θ_e.

In (El Murr et al., 2007, a; El Murr et al., 2008, b; El Murr et al., 2008, c; BelHadj Brahim et al., 2013, d), the position extraction can be based on:

- A conventional Phase Locked Loop (PLL),
- Short Time Fourier Transform (STFT) ridges.

The first algorithm based on the conventional PLL scheme is strongly dependent on some machine parameters, and the estimated position and speed response can be detected from the actual position at certain operating conditions.

The second algorithm is machine parameters independent and even more efficient than the PLL under any condition. However, its real time implementation is complicated and requires a lot of calculation.

To overcome these two algorithms drawbacks, a modified SHF current demodulation scheme is proposed in the next subsection.

4.2 The Modified SHF current demodulation algorithm

The modified SHF current demodulation algorithm principle is presented in Fig.4. The proposed modification gives some significant advantages compared with the two reported algorithms. In fact, the modified algorithm presents an easier tuning of the filters needed in the demodulation stage, and then allows the elimination of the conventional PLL and the STFT ridges solutions. This will help to increase the dynamic performance of the position estimation.

Both currents i_1 and i_2 are filtered using two low pass filters (LPF). The expressions of the low-pass filtered currents, noted respectively i_{1LPF} and i_{2LPF} are given by (29) and (30).

$$i_{1LPF} = LPF(i_1) = i_{cp} i_{cn} \sin(2\theta_e) \quad (29)$$

$$i_{2LPF} = LPF(i_2) = -i_{cp} i_{cn} \cos(2\theta_e) \quad (30)$$

Finally, the magnetical position can be extracted according to (31) thanks to the "atan2 CORDIC" function applied to the currents i_{1LPF} and i_{2LPF}. Indeed, this function allows position calculation even if the i_{2LPF} value is around zero.

$$2\hat{\theta}_e = \pi - a\tan 2\left(\frac{i_{1LPF}}{i_{2LPF}}\right) \quad (31)$$

Thus, the electrical position can be easily performed.

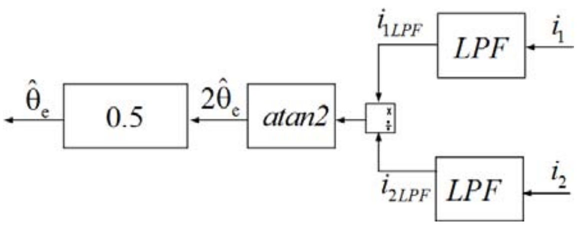

Fig. 4. The modified IPMSM rotor position extraction based on the modified SHF current demodulation scheme.

4. SIMULATION AND EXPERMENTAL RESULTS

In order to test the performance of the modified SHF current demodulation scheme for the rotor position estimation at low speeds and standstill, simulations and experimental tests have been performed in Open Loop conditions under different speeds using a three-phase IPMSM, designed for washing machines. The IPMSM parameters, considered for performing simulations, are given in the appendix.

The injected high frequency voltages magnitude and frequency have been set respectively to 57V and 1kHz according to a previous study detailed in (BelHadj Brahim et al., 2011, a).

Then, the HPF cut-off frequency is chosen to be 800Hz. Moreover, the LPF cut-off frequency is chosen to be 100Hz since the position information is related to low speeds and standstill.

On the other hand, the results presented in this section have been obtained taking into account first that the washing machine drum operates at low speeds and second that the drum speed rotation must be reversed for every few turns of the machine washing cycle.

In fact, typical range of drum speed is [30 ; 45rpm] and [-30 ; -45rpm], (Balazovic et al., 2008; Andreescu, 2003).

5.1 Simulation results

The simulations carried out to test the proposed position estimator performance have been executed under MATLAB/Simulink® software environment at low speeds and standstill.

<u>Simulation results at low speeds at no load IPMSM conditions</u>:

The simulation estimated positions obtained in Open Loop conditions at different low speeds and with no load, are presented in Fig.5. As the required speed should be chosen in the low speed range, then the IPMSM speed control is reported in steady state considering a speed reference respectively of 120rpm, 80rpm and 40rpm, which corresponds to a supply frequency f_e respectively of 6Hz, 4Hz and 2Hz.

Fig.5 presents the IPMSM actual and estimated electrical positions. The simulation results show good agreement between actual and estimated positions at low speeds. In fact, the absolute position error obtained is of 3°.

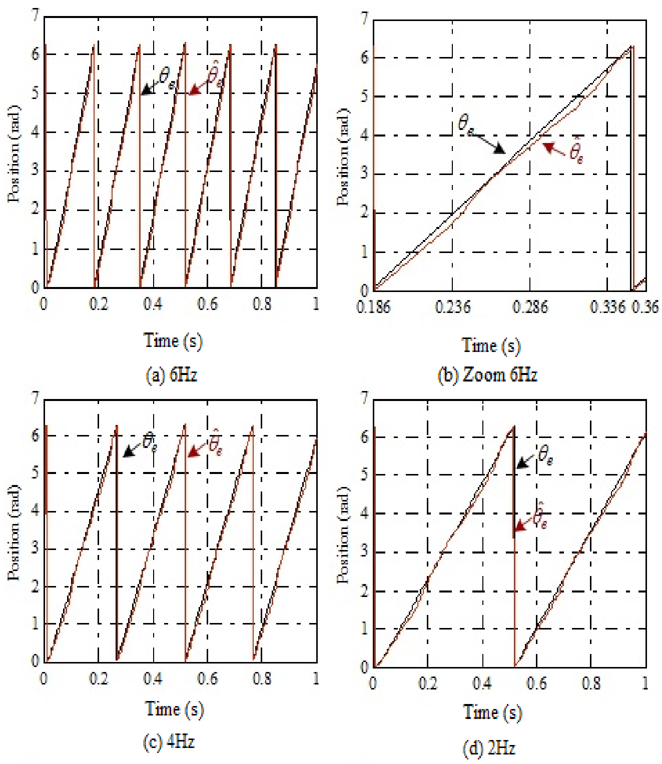

Fig. 5. Actual and estimated electrical positions. No loaded IPMSM.

Simulation results at low speeds at loaded PMSM conditions:

Other simulations have been carried out in the low speed range in Open Loop control conditions considering different load levels. The IPMSM speed reference has been set to 120rpm. Four load levels have been considered, which are respectively 25%, 50%, 75% and 100% of the nominal electromagnetic torque C_n.

The load torque have been applied at time t=0.4s.

Both actual and estimated electrical positions obtained for these load levels are presented in Fig.6.

Fig.7.a shows the speed reference applied to the IPMSM drive. The IPMSM operates initially at 40rpm with ful load condition. At time t = 1s, the speed reference was reversed at the same load condition. The corresponding IPMSM speed is then given by Fig.7.b. The resulted actual and estimated electrical position are presented in Fig.7.c.

The simulation results show good agreement between actual and estimated positions at ful load condition even if the rotation is reversed.

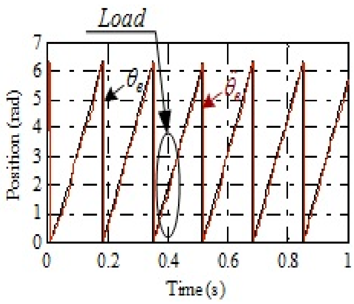

(a) 25% loaded IPMSM.

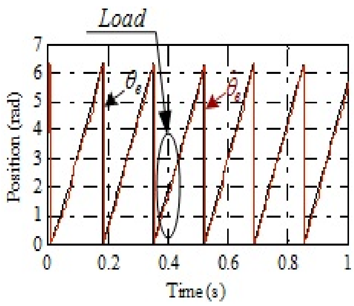

(b) 50% loaded IPMSM.

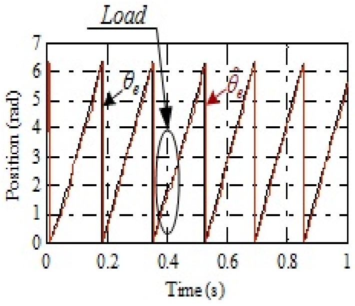

(c) 75% loaded IPMSM.

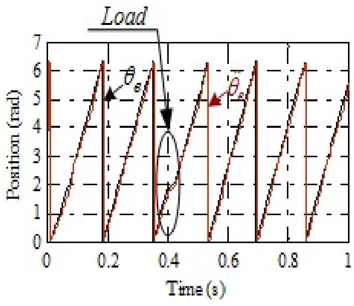

(d) 100% loaded IPMSM.

Fig. 6. Actual and estimated electrical positions. Loaded IPMSM supplied at $f_e = 6Hz$.

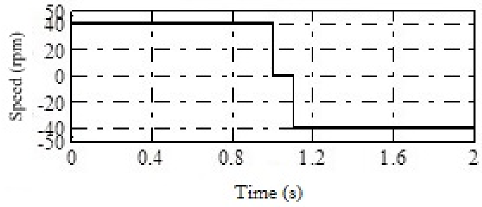

(a) Speed reference.

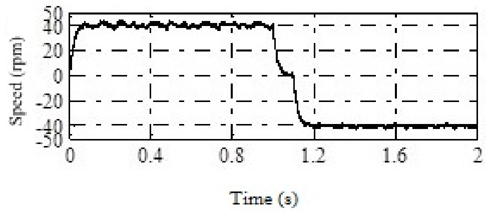

(b) Actual speed.

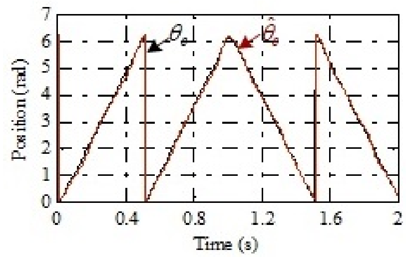

(c) Actual and estimated electrical positions.

Fig. 7. IPMSM variables : (a)Speed reference, (b)Actual speed, (c) actual and estimated electrical positions. 100% loaded IPMSM supplied at $f_e = 2Hz$.

Simulation results at standstill:

This subsection deals with the electrical position estimation at standstill with no loaded IPMSM.

As the IPMSM is a 3-pole pairs motor, its electrical period is of 120°. Then an electrical period corresponds to the third of a mechanical period. Fig.8 presents the estimated electrical position as a function of the actual electrical position at standstill under no load condition. The step position precision used in this test is fixed at 2°.

The simulation result presented in Fig.8 shows good agreement between actual and estimated electrical position at standstill with an average position error of 5°.

The following subsection presents the experimental results obtained for the same IPMSM drive in order to validate the obtained simulation results.

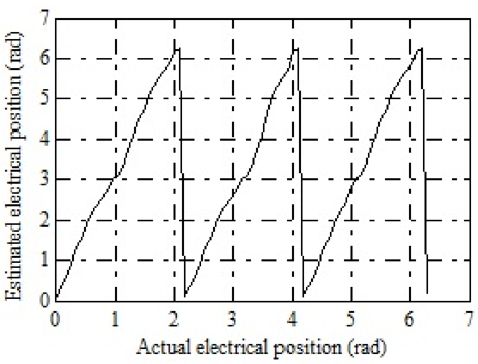

Fig. 8. Estimated electrical position at standstill. No loaded IPMSM.

5.2 Experimental results

An experimental setup has been developed in order to validate the simulation results obtained with the modified IPMSM rotor position extraction considering the SHF current demodulation scheme based AVI technique at low speeds and standstill conditions. The experimental setup, Fig.9, is composed of:

- A three-phase IPMSM, designed for washing machines.
- A dsPICDEMTM MC1H three-Phase High Voltage Power Module optimized for three-phase motor applications that require DC bus voltages up to 400V and can deliver up to 1kW power output. This power module integrated a power inverter and a three Hall-effect current sensors. It operates directly from the AC line voltage. The switching frequency of the inverter is 20kHz. It is important to note that for this domestic application, the DC link voltage is set to 325V.
- A dsPICDEMTM MC1 Motor Control Development Board based on 16-bit fixed-point dsPIC30F6010A with 7.3728MHz as external clock frequency. The analog digital converter ADC associated to this dsPIC is a 10-bits converter.

Both space vector PWM algorithm, used for the motor control, and AVI technique algorithm are implemented on the dsPIC30F6010A of the dsPICDEM Board. The AVI technique is based on the use of a digital first-order high-pass IIR filter, in order to recover the HF current components i_{sdc} and i_{sqc}, and a digital first-order low-pass IIR filter in order to extract the electrical rotor position. Indeed, the high frequency signal was injected by modulation of PWM signals sent to the inverter.

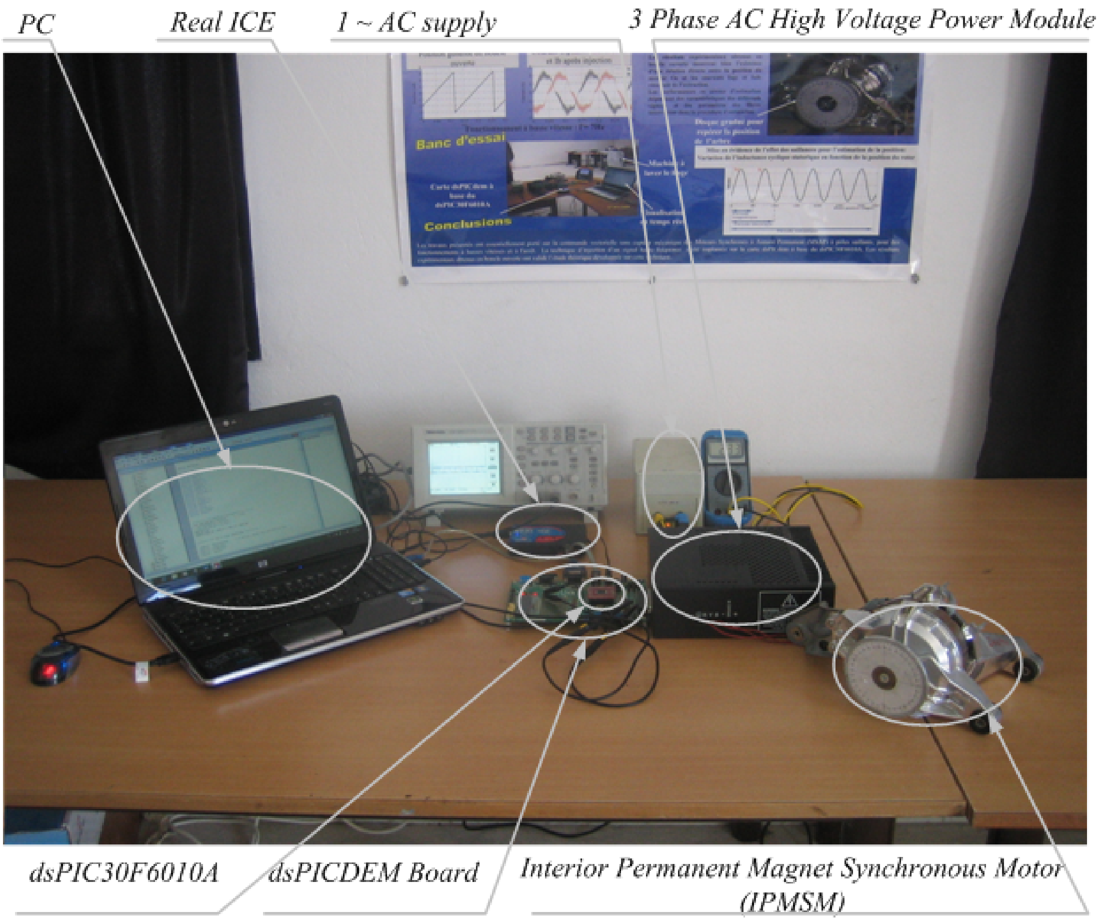

Fig. 9. Experimental setup.

Fig.10 shows a view of the IPMSM associated to a position-graduated disk mounted on the IPMSM axis.

Fig.10.a shows the position-graduated disk used to fix the IPMSM position at standstill. The black arc presents an electrical period of [0 120°]. The position precision offered by the disk is of 2°.

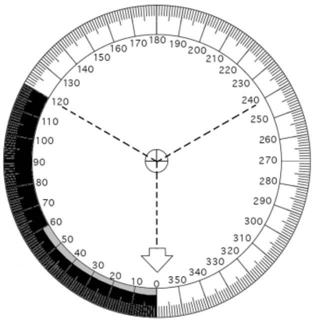

(a) Disk

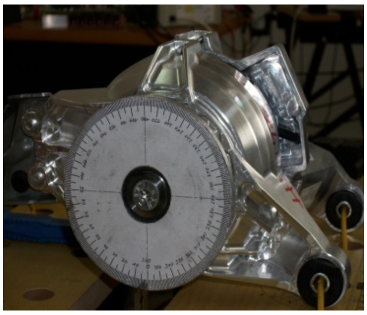

(b) Position-graduated disk associated to the PM!

Fig. 10. Position-graduated disk mounted on the IPMSM.

The experimental estimated positions obtained in Open Loop conditions at different low speeds and with no load, are presented in Fig.11. The IPMSM control reference speeds are respectively 120rpm, 80rpm and 40rpm, which correspond to a supply frequency f_e respectively of 6Hz, 4Hz and 2Hz.

Fig.11 shows that the Alternating Voltage Injection (AVI) technique based on modified SHF current demodulation algorithm is able to estimate the rotor position of IPMSM at low speeds.

<u>Experimental results at standstill</u>:

Fig.12 presents the estimated electrical position as a function of the actual electrical position at standstill under no load condition. The position precision used in this test is fixed at 2°.

The experimental result presented in Fig.12 shows good agreement between actual and estimated electrical position at standstill with an average position error of 2°.

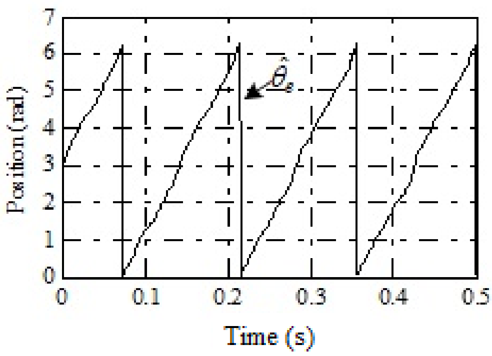

(a) 6Hz

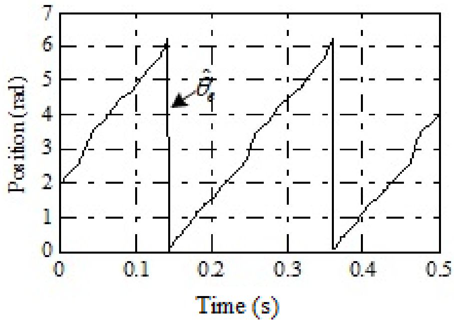

(b) 4Hz

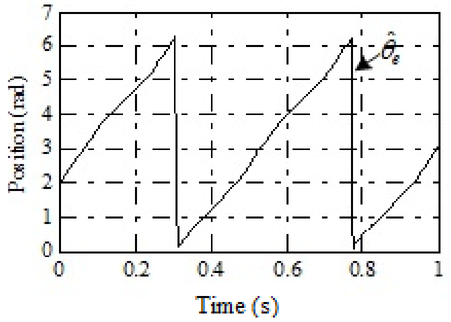

Fig. 11. Experimental estimated electrical positions. No loaded IPMSM.

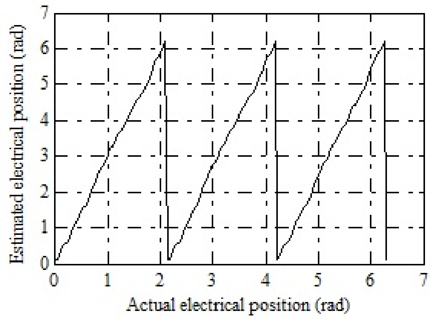

Fig. 12. Experimental estimated electrical position at standstill. No loaded IPMSM.

6. CONCLUSION

A modified Shifted High Frequency current demodulation scheme based Alternating Voltage Injection technique sensorless control for an Interior Permanent Magnet Synchronous Motor is proposed to overcome the drawbacks of other proposed high frequency currents demodulation algorithms in the literature. The modified algorithm offers an easier tuning of the filters, and also an elimination of the conventional Phase Looked Loop and Short Time Fourier Transform (STFT) ridges. This allows reducing the hardware necessary to the real time rotor position sensorless technique implementation.

Simulations and experimental results have proved that the modified Shifted High Frequency current demodulation scheme is able to estimate the IPMSM rotor position at low speed ranges and standstill. The use of the modified algorithm has resulted in position estimation with an average position error of 2° at standstill under no load condition.

The modified algorithm based rotor position estimation can be conveniently implemented in Closed Loop control conditions in order to improve the position estimation and thus the IPMSM sensorless control performance.

ACKNOWLEDGMENT

This research project was supported by the Tunisian Ministry of High Education and Scientific Research under Grant LSE-ENIT- LR 11ES15 and by APPCON Technologies company.

APPENDIX 1. IPMSM PARAMETERS

Variable	Designation	Value
Rated power	P_n	1kW
Rated torque	C_n	0.7 N.m
Rated speed	N_n	1000 rpm
Rated current	I_n	2.6 A
Pairs poles Number	p	3
Rotor magnet flux	ψ_f	0.0705Wb
Stator Resistance	R_s	2.4 Ω
d and q-axis magnetizing inductances	L_{sd} , L_{sq}	11.9, 14.2 mH

REFERENCES

Andreescu, G.D. (2003). Sliding-mode Observer for Sensorless Control of Permanent Magnet Synchronous Motor Drives. *Journal of Control Engineering and Applied Informatics, CEAI*, Vol (5), no. 1, pp. 27-34.

Balazovic, P. and Filka, R. (2008). Sensorless PMSM control for H-axis washing machine drive. *In Proc. IEEE Power Electronics Specialists Conference, PESC*, pp. 4237-4242.

BelHadj Brahim, O., Ben Attia Sethom, H., Sammoud, H. and Slama Belkhodja, I. (2011). Optimized High Frequency Signal Injection Based Permanent Magnet Synchronous Motor Rotor Position Estimation Applied to Washing Machines. *American Journal of Engineering and Applied Sciences*, vol (4), no. 3, pp. 390-399.

BelHadj Brahim, O., Ben Attia Sethom, H., Sammoud, H. and Slama Belkhodja, I. (2011). Continuous HFSI Technique Applied to Rotor Position Estimation of IPMSM at Standstill and Low Speed-A Survey. *In Proc. IEEE, 8th International Multi Conference on Systems, Signals & Devices, SSD'11,* pp. 1-10.

BelHadj Brahim, O., Ben Attia Sethom, H., Sammoud, H. and Slama Belkhodja, I. (2012). AVI Demodulation Schemes for IPMSM position estimation at standstill and low speed-A Review. *Transactions on Systems, Signals &* Devices, Issues on Power Electrical Systems, vol (7), no. 2, pp.1-18.

BelHadj Brahim, O., Ben Attia Sethom, H., Sammoud, H. and Slama Belkhodja, I. (2013). A Modified AVI Technique Demodulation Scheme Based IPMSM Sensorless Control at Low Speeds and Standstill. *In Proc. IEEE, 10th International Multi Conference on Systems, Signals & Devices, SSD'13*.

Chaudhary, M.P., Patel, V. and Jamnani, J.G. (2008). Sensorless vector control of PMSM drive using heterodyne technique. *In Proc. IEEE Optimization of Electrical and Electronic Equipment International Conf.,* pp. 93-99.

Chen, J.-L., Tseng, S.-K. and Liu, T.-H. (2012). Implementation of high-performance sensorless interior permanent-magnet synchronous motor control systems using a high-frequency injection technique. *IET Electric Power Applications,* vol (6), no. 8, pp. 533-544.

De Belie, F.M.L., Sergeant, P. and Melkebeek, J.A. (2010). A sensorless drive by applying test pulses without affecting the average-current samples. IEEE Trans. Power Electron., vol (25), no. 4, pp. 875-888.

El Murr, G., Giaouris, D. and Finch, J.W. (2007). Sensorless Speed Estimation of PMSM near Zero Speed Using Online Short Time Fourier Transform Ridges. *In Proc. the World Congress on Engineering,* vol (I).

El Murr, G., Giaouris, D. and Finch, J.W. (2008). Universal PLL strategy for sensorless speed and position estimation of PMSM. *IEEE International Industrial and Information Systems Conf.,* pp.1-6.

El Murr, G., Giaouris, D. and Finch, J.W. (2008). Totally Parameter Independent Speed Estimation Of Synchronous Machines Based On Online Short Time Fourier Transform ridges. *International Association of Engineers, Engineering Letters, 16:1, EL 16 1 14,* vol (16), no. 1.

Foo, G. and Rahman, M.F. (2010). Sensorless vector control of interior permanent magnet synchronous motor drives at very low speed without signal injection. *IET Electric Power Applications,* vol (4), issue3, pp. 131-139.

Hua, Y., Sumner, M., Asher, G., Gao, Q. and Saleh, K. (2011). Improved sensorless control of a permanent magnet machine using fundamental pulse width modulation excitation. *In Proc. IET Electric Power Applications,* vol (5), no. 4, pp. 359-370.

Silva, C., Asher, G.M., Sumner, M. and Bradley, K.J. (2003). Sensorless rotor position control in a Surface Mounted PM Machine using HF rotating injection. *EPE Journal,* vol (13), no. 3.

Villet, W.T., Kamper M.J., Landsmann, P. and Kennel, R. (2012). Evaluation of a simplified high frequency injection position sensorless control method for reluctance synchronous machine drives. *In Proc. 6th IET International Conference on Power Electronics, Machines and Drives, PEMD,* pp. 61.

Wang, C. and Xu, L. (2004). A novel approach for sensorless control of PM machines down to zero speed without signal injection or special PWM technique. *IEEE Trans. Power Electron.*, vol (19), no. 6, pp. 1601-1607.

Wang, H.-B. and Liu, H.-P. (2009). A novel sensorless control method for brushless DC motor. *IET Electric Power Applications,* vol (3), no. 3, pp. 240-246.

Wallmark, O., Gali_c, J. and Mosskull, H. (2012). Sensorless control of permanent-magnet synchronous motors adopting indirect self-control. *IET Electric Power Applications,* vol (6), no. 1, pp. 12-18.

Yousfi, D. and Darkawi, A. (2008). Comparison of two position and speed estimation techniques used in PMSM sensorless vector control. *In Proc. 4th IET International Conference on Power Electronics, Machines and Drives, PEMD*, pp. 626-630.